Available online at www.sciencedirect.com

SciVerse ScienceDirect

Ceramics International 39 (2013) 969–976

CERAMICS INTERNATIONAL

www.elsevier.com/locate/ceramint

Preparation of porous Y_2SiO_5 ceramics with relatively high compressive strength and ultra-low thermal conductivity by a TBA-based gel-casting method

Zhenguang Hou, Jiachen Liu*, Haiyan Du, Hai Xu, Anran Guo, Min Wang

School of Materials Science and Engineering of Tianjin University, Key Laboratory of Advanced Ceramics and Machining Technology of Ministry of Education, Tianjin 300072, China

Received 27 May 2012; received in revised form 28 June 2012; accepted 4 July 2012
Available online 14 July 2012

Abstract

Porous Y_2SiO_5 ceramics with relative high compressive strength (as high as 24.45 MPa) and ultra-low thermal conductivity (~0.08 W/m K) were successfully fabricated by a tert-butyl alcohol based gel-casting method. The formation mechanism of the 3D interconnected pores and the properties of the green body are discussed. The porosity, pore size, compressive strength and thermal conductivity could be controlled by varying the initial solid loading and the sintering temperature. When regulating the initial solid loading (from 20 to 50 wt%) and sintering temperature (from 1200 to 1500 °C), the porosity can be controlled between 47.74% and 73.93%, and the compressive strength and the thermal conductivity of porous Y_2SiO_5 ceramics varied from 3.34 to 24.45 MPa and from 0.08 to 0.55 W/m K, respectively. It should be noted that the porous Y_2SiO_5 ceramics with 30 wt% solid loading and sintering at 1400 °C had an open porosity of 61.80%, a pore size of 2.24 μm, a low room-temperature thermal conductivity of 0.17 W/m K and a relatively high compressive strength of 13.91 MPa, which make this porous Y_2SiO_5 ceramics suitable for applications in high-temperature thermal insulators.

Keywords: TBA-based gel-casting; Y_2SiO_5; Compressive strength; Thermal conductivity

1. Introduction

Yttrium silicate (Y_2SiO_5) ceramic is an interesting structural material [1] and a number of published works have focused on its coating applications [2–8], which is mainly due to its two important features. Firstly, the thermal expansion coefficient of Y_2SiO_5 ($(8.36 \pm 0.5) \times 10^{-6}\,K^{-1}$) matches well with those of most non-oxide ceramics [9,10]. Secondly, the low evaporation rate of Y_2SiO_5 along with its low oxygen permeability constant at temperature up to 1900 °C endows this ceramic with excellent oxidation resistance [11]. Recently, Sun et al. [11–13] have prepared single-phase Y_2SiO_5 by a solid–liquid reaction method at a relatively low temperature (1500 °C) with a short holding time (2 h) by introducing a $LiYO_2$ additive and investigated the mechanical and thermal properties of Y_2SiO_5 ceramics. It was found that the thermal conductivity of Y_2SiO_5 (1.86 and 1.29 W/m K at 300 K and 1400 K, respectively) was much lower than that of most commonly used thermal barrier coating materials (such as YSZ, $La_2Zr_2O_7$, etc.), which makes it very competitive as a thermal insulation material.

Porous ceramics have been of considerable interest and technical importance due to their extensive applications, including supports for catalysts, artificial bones, filters, chemical sensors and light-weight thermal insulation parts [14–18]. The advantages of using porous ceramics are usually high porosity, large surface area, low density and low thermal conductivity which can be tailored by controlling the microstructure of pores according to specific applications [19–22]. A number of processing techniques for the production of porous ceramics have been developed, including replica, sacrificial template, direct foaming, freeze casting and water-based gel-casting [23–26]. As a new method, the

*Corresponding author. Tel.: +86 13622049265; fax: +86 022 27408244.
E-mail address: jcliutju@gmail.com (J. Liu).

0272-8842/$36.00
http://dx.doi.org/10.1016/j.ceramint.2012.07.014

TBA-based gel-casting process is a recently developed method for fabrication of porous ceramics [27]. Porous ceramics with ultra-high porosity could be achieved by use of the ultra-low solid loading of slurries in this method. This is owing to the high saturation vapor pressure and low surface tension force of tert-butyl alcohol (TBA). Compared with water, TBA can evaporate easily under relatively low temperatures (40 °C). Furthermore, the properties of porous ceramics produced by this technique could be adjusted directly by changing the solid loading in the slurry and the sintering temperature [28,29]. The most important features of porous ceramics fabricated by this method are the uniformly distributed pores and unique 3D-framework structures [14,30–32]. As a potential thermal insulation material, however, there is no experimental data in literature for the preparation of porous Y_2SiO_5 ceramics by this method.

As the single-phase Y_2SiO_5 powder is not commercially available, the single-phase Y_2SiO_5 should be prepared in advance. The main aim of the present work was to explore the application of the TBA-based gel-casting method to prepare highly porous Y_2SiO_5 ceramics with relative high compressive strength and ultra-low thermal conductivity. The effects of initial solid loading and sintering temperature on the microstructure and properties of green bodies and final sintered Y_2SiO_5 ceramics were investigated. The results obtained in this paper are beneficial to the promotion of the porous Y_2SiO_5 material as a candidate for high-temperature and light-weight insulators.

2. Experimental procedure

2.1. Raw materials

Y_2O_3 powder (Changsha Deli Rare earth Chemical Co., Ltd., China) and SiO_2 powder (Zhejiang Tongda Weipeng Electric Co., Ltd., China) were used as the starting materials. Tert-butyl alcohol (TBA) was used as the shaping solvent and pore forming agent in the gel casting process. A premix solution was prepared in TBA with the monomer (acrylamide, AM, $C_2H_3CONH_2$) and the cross linker (N,N-methylenebisacrylamide, MBAM, $(C_2H_3CONH)_2 \cdot CH_2$). Ammonium persulfate (APS) and N,N,N,N-tetramethylethylenediamine (TEMED) were selected as the initiator and catalyst for gelation reaction, respectively. Citric acid was used as the dispersant (1 wt% of the Y_2SiO_5 powder) to form stable Y_2SiO_5 suspensions in TBA. All chemicals used in this study were of analytical (AR) grade.

2.2. Fabrication procedure

Fig. 1 shows a detailed process scheme for the preparation of Y_2SiO_5 powder by the solid–liquid reaction method and porous Y_2SiO_5 ceramics by TBA-based gel-casting. The Y_2O_3 and SiO_2 powders (molar ratio 1:1) were calcined at different temperatures (1400, 1450, and 1500 °C) for 2 h to find the appropriate temperature to synthesize single-phase Y_2SiO_5. The Y_2SiO_5 powder was ground in ethanol for 10 h to break up agglomerates and reduce the particle size.

For the present study, the weight ratio was AM:MBAM:TBA = 12:1:50. Slurries with different solid loadings (20, 30, 40 and 50 wt%) were prepared by ball milling the Y_2SiO_5 powder in the premix solution for 4 h. The prepared slurries were found to be stable and had good flow ability for casting. Then, appropriate amounts of initiator and catalyst solutions were added into the suspension to induce polymerization of the monomers. The slurries were immediately poured into polyethylene molds and placed in an oven at 40 °C. The green bodies were removed from the molds and dried at a temperature of 40 °C for 12 h. Finally, the dried samples were sintered at different temperatures from 1200 to 1500 °C for 2 h. The

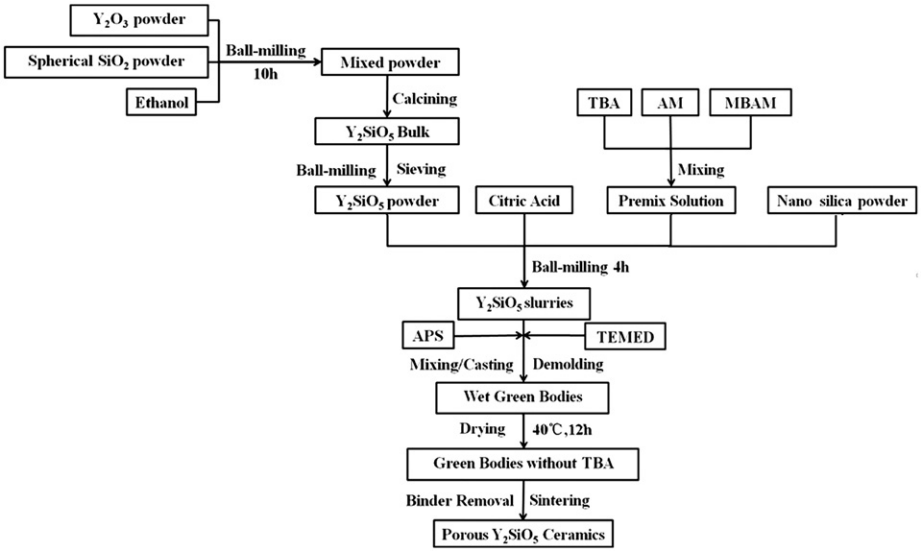

Fig. 1. Technological process scheme for the preparation of Y_2SiO_5 powder by the solid–liquid reaction method and porous Y_2SiO_5 ceramics by TBA-based gel-casting.

sintering regime entailed heating the samples at 2 °C/min up to 600 °C followed by 1 h of holding time, and then heated at 5 °C/min up to the final sintering temperature.

2.3. Characterization

The synthesized Y_2SiO_5 powder was characterized by XRD (CuKα radiation, D/Max-2500 Rigaku, Japan) from 10° to 60° with a scanning speed of 2 °/min. Open porosities and densities of the sintered samples were determined by the water-immersion technique using the Archimedes method. The density of dried green bodies was calculated from the mass and dimension of samples. The compressive strength was measured by a universal testing machine (XWW, Beijing Shengxin detecting instrument, China) with a crosshead speed of 0.5 mm/min. The green samples were cylindrical, 10–12 mm in diameter and 20 mm in height, and the dimensions of sintered specimens were according to the different shrinkages. The linear shrinkage of samples during drying and sintering processes was determined by the following equation: shrinkage $=[(l_a-l_b)/l_a]\times 100\%$, where l_a and l_b are the diameter of initial samples and dried or sintered samples, respectively. Thermal conductivity at room temperature was measured by the thermal-conductivity instrument (C-3000, Xian Xiaxi Electric Co., Ltd., China). The dimensions of measured samples were 30 mm diameter and 5 mm height. Each value represented an average of five measurements of five different specimens. Micrographs of the fracture surface of sintered samples were observed with a scanning electron microscope (S-4800, Hitachi Ltd., Japan). The pore size distribution was measured by an automatic mercury injection apparatus (IV9500, Micromeritics Instrument Corporation, USA).

3. Result and discussion

3.1. Characterization of synthesized Y_2SiO_5 powder

XRD patterns of the synthesized Y_2SiO_5 powder calcined at different temperatures varying from 1400 to 1500 °C are illustrated in Fig. 2. After calcining at 1400 °C for 2 h [Fig. 2(b)], all characteristic peaks corresponding to Y_2SiO_5 (JCPDS card # 36-1476) were confirmed to be present, accompanied by a large amount of Y_2O_3 and SiO_2. This result demonstrated that the reaction between yttrium and silica was insufficient. The content of Y_2O_3 decreased when the temperature increased to 1450 °C [Fig. 2(b)]. Furthermore, the XRD results [Fig. 2(c)] indicated that the powder calcined at 1500 °C was pure single-phase Y_2SiO_5 which is consistent with the standard patterns of Y_2SiO_5 [Fig. 2(a)]. Therefore, the Y_2SiO_5 powder synthesized at 1500 °C for 2 h was used to prepare the porous ceramics. The single-phase Y_2SiO_5 powder after grinding in ethanol had an average particle size of 1.91 μm and a narrow particle size distribution. Fig. 3 shows a SEM micrograph of the Y_2SiO_5 powder for preparing

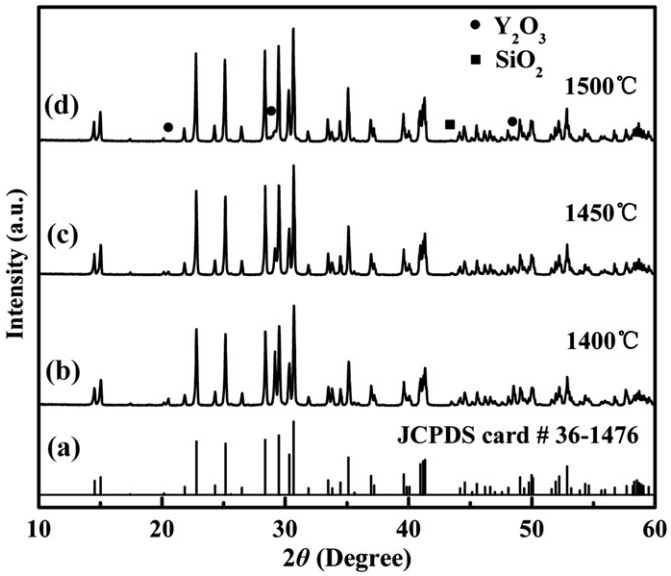

Fig. 2. XRD patterns of Y_2SiO_5 powder synthesized at different temperatures for 2 h in air: (a) Standard pattern of Y_2SiO_5; (b) 1400 °C; (c) 1450 °C; (d) 1500 °C.

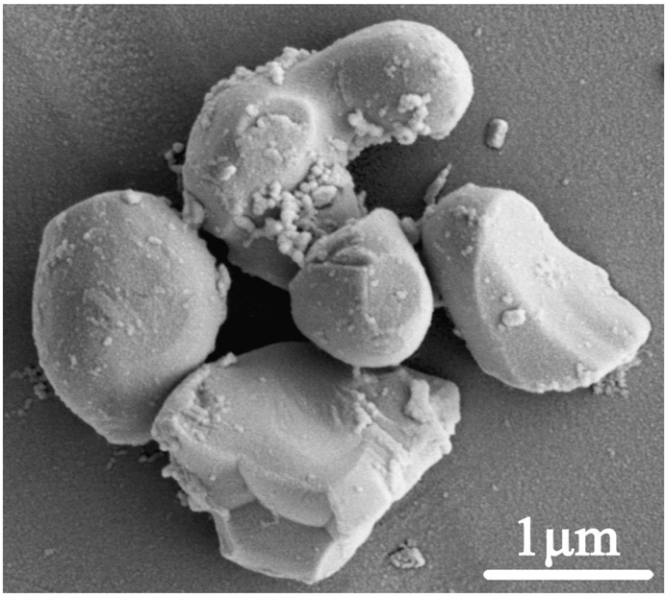

Fig. 3. SEM micrograph of Y_2SiO_5 powder.

Y_2SiO_5 slurries. It can be clearly seen that the diameter of the particles is 1–2 μm and the shape is approximately spherical.

3.2. Properties of the green bodies with different solid loadings

The pore forming schematic diagram of porous Y_2SiO_5 ceramics by TBA-based gel-casting is shown in Fig. 4. After adding appropriate amounts of initiator and catalyst solution into the stable Y_2SiO_5 slurry [Fig. 4(a)], the polymerization of AM occurred in several minutes. The

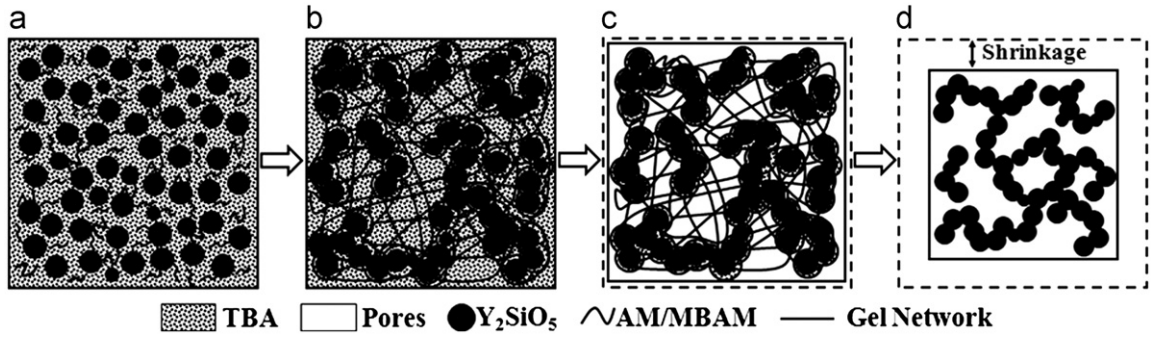

Fig. 4. Pore forming schematic diagram of porous Y_2SiO_5 ceramics by TBA-based gel-casting.

formed strong macromolecular gel network trapped Y_2SiO_5 particles in its branches, and the green body was obtained without any shrinkage [Fig. 4(b)]. Then most of the TBA vaporized from the Y_2SiO_5 ceramics bodies, leaving many pores during the drying process at 40 °C. The pores connected with each other and distributed homogeneously throughout the dried body. Meanwhile, the particles would approach each other to support the structure, thus leading to a small shrinkage of green bodies [Fig. 4(c)]. After sintering, the polymer and residual TBA were removed completely and the Y_2SiO_5 particles interconnected with each other, forming a loose skeleton structure [Fig. 4(d)]. The linear shrinkage of the specimens after drying was around 1.52–10.67%, which was mainly due to the ultra-low solid loading. And the linear shrinkage of samples would decrease as the solid loading increased. In addition, there were no obvious cracks observed on the surface of green bodies. Fig. 5 shows the properties of green bodies with different solid loadings varying from 20 to 50 wt%. It was observed that after drying, the bulk density (1.02–2.20 g/cm^3) of all the green bodies was far less than the theoretical density of Y_2SiO_5 (4.44 g/cm^3). What is more, Fig. 6(a) reveals the typical porous microstructure of the green body with 30 wt% solid loading after evaporation of TBA. It indicates that the pores originating from the evaporation of TBA were retained in the dried samples. Though a lower solid loading would result in a higher porosity, it should be noted that it is not appropriate to decrease the solid loading to lower than 20 wt% in this work. If the solid loading was lower than 20 wt%, the particles could not connect with each other to support the framework after the organics were burned out. After polymerization, the strength of the green bodies was greatly improved. Even if the solid loading was as low as 20 wt%, the compression strength was as high as 4.51 MPa, which was strong enough to hand and machine the production before sintering. In the meantime, with increasing solid loading, the compressive strength increased from 4.51 to 25.39 MPa. It can be clearly seen from Fig. 6(b) that the suspended Y_2SiO_5 particles formed agglomerations with dimensions of about 1 μm and were locked by polyacrylamide, creating a rigid 3D skeleton structure, which was

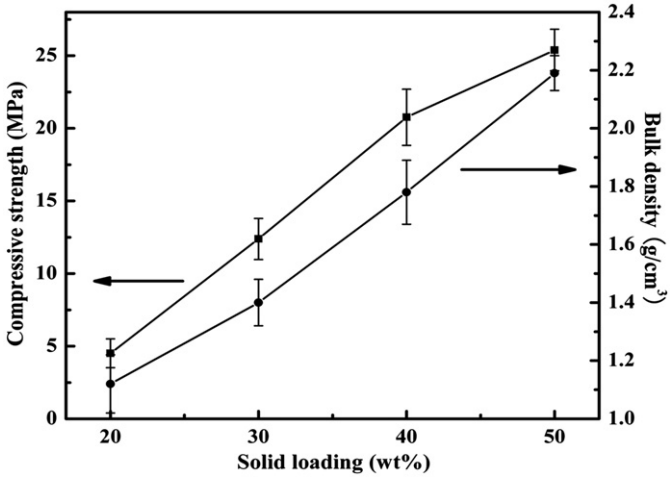

Fig. 5. Properties of green bodies with different solid loadings varying from 20 wt% to 50 wt%.

responsible for the high compressive strength of green bodies.

3.3. Effect of sintering temperature on sintered samples

The effects of sintering temperature on porosity and bulk density were investigated and the results are shown in Fig. 7. The evolution of microstructure of samples with 30 wt% solid loading during sintering is shown in Fig. 8(a)–(d). It can be concluded that with a given solid loading (30 wt%), the sintering temperature significantly affected the changes of porosity and pore size. As the sintering temperature increased from 1200 to 1500 °C, the porosity of porous Y_2SiO_5 ceramics with 30 wt% solid loading decreased from 67.09% to 58.31%, while the bulk density increased accordingly from 0.99 to 1.32 g/cm^3. Fig. 9(a, b) shows the pore size distribution and cumulative pore volume of the samples sintered at different sintering temperatures. After sintering, all samples presented a single peak with narrow half-peak width (from 0.5 to 3 μm), suggesting a uniform pore size distribution. It was noticed that the mean pore size generally decreased from 2.90 to 2.17 μm with increasing sintering temperature from 1200 to 1500 °C [Fig. 9(a)]. The total cumulative volume

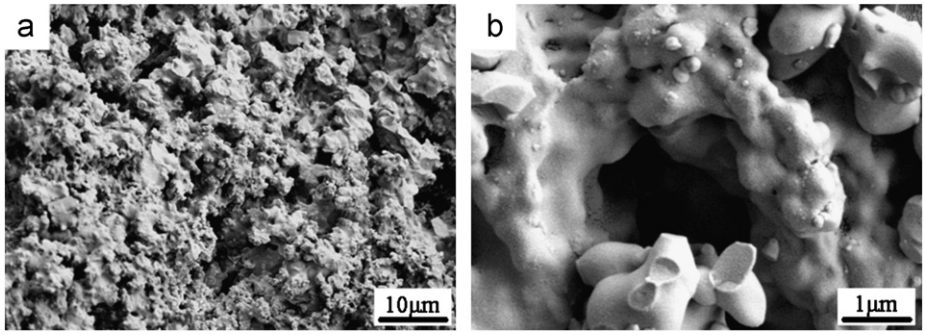

Fig. 6. (a) Microstructure of green body from slurry with 30 wt% solid loading; (b) typical connections of Y_2SiO_5 particles in green bodies.

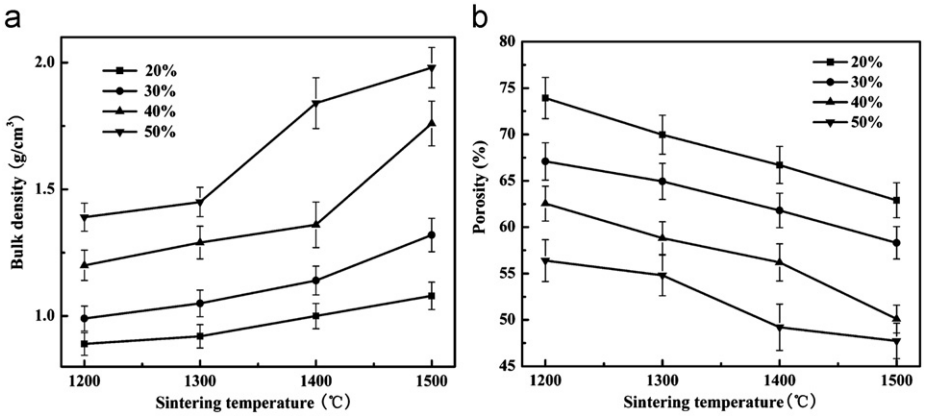

Fig. 7. Variation of bulk density (a) and porosity (b) of porous Y_2SiO_5 ceramics with sintering temperature and solid loading.

generally decreased with increasing temperature, which is consistent with the porosity–temperature dependence [Fig. 7(a)]. Moreover, the cumulative volume of open pores in the sample sintered at 1500 °C increased more steeply than that of the sample sintering at 1200 °C. This suggests that, with increasing sintering temperature, the smaller pores (from 0.5 to 1 μm) were eliminated, resulting in a somewhat narrower pore size distribution. It should be noted that the linear shrinkage of samples with 30 wt% solid loading increased from 9.69% to 18.85% as the sintering temperature increased from 1200 to 1500 °C. The shrinkage after sintering was mainly caused by the transition of agglomerations to large crystal grains and then the connection of crystal grains at the neck [Fig. 8(f)]. It can be concluded from Fig. 8(e, f) that the most important characteristics of porous Y_2SiO_5 ceramics by this method are the uniform distributed interconnected pore structure and typical 3D framework.

Fig. 10 shows the effect of sintering temperatures on the compressive strength and room-temperature thermal conductivity. It demonstrated that the compressive strength increased from 3.34 to 16.51 MPa when the sintering temperature increased from 1200 to 1500 °C. It can be observed that the particles of the sample sintered at 1200 °C were loosely lapped with each other with few connections, which resulted in a lower compressive strength (3.34 MPa). When the temperature further increased, adjacent particles interconnected, forming a strong neck, finally leading to the increase of the compressive strength. Highly porous ceramics fabricated by conventional methods often contain defects, such as cracking and surface flaws [28]. These defects in the cell structure would significantly reduce the strength of porous ceramics. However, there were no noticeable defects and cracks in the samples prepared by TBA-based gel-casting [Fig. 8(e)], which indicated that the sintering process did not cause any destruction of the pore structure. This might be another important reason for the high compressive strength. It can be seen from Fig. 10 that all the samples had low thermal conductivities from 0.13 to 0.20 W/m K, which were much lower than that of fully dense Y_2SiO_5 ceramics (~1.86 W/m K). This was mainly attributed to the unique 3D interconnected pore structures within the porous Y_2SiO_5 ceramics. Firstly, the large number of air-filled pores prevented the heat transfer along the direction of thickness because the thermal conductivity of air (0.026 W/m K) was much lower than that of Y_2SiO_5. Secondly, the interconnected pores in the matrix made the ceramics grains not necessarily continuous or dispersed, blocking the heat conducting pathways.

3.4. Effect of solid loading on sintered samples

It was noted that the microstructure and properties of porous Y_2SiO_5 ceramics were also significantly influenced

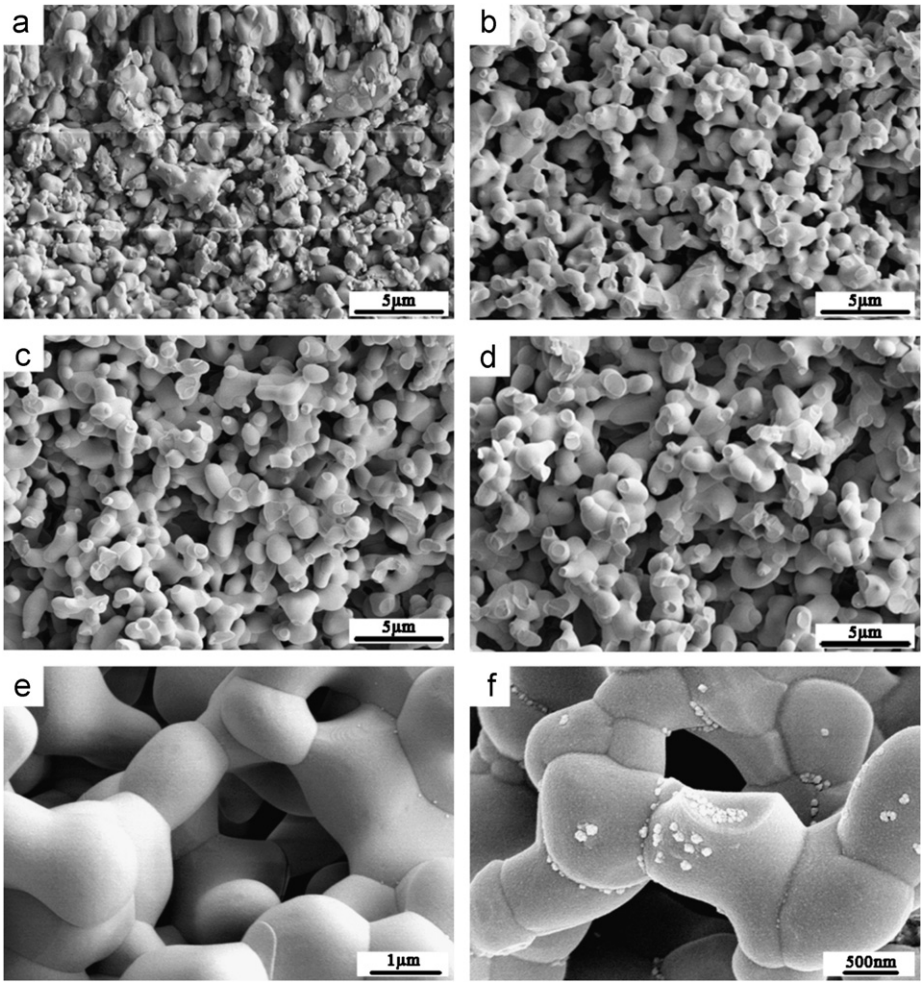

Fig. 8. Details of 3D-interconnection of pores in the samples with 30 wt% solid loading sintering at different temperatures: (a) 1200 °C; (b) 1300 °C; (c) 1400 °C; (d) 1500 °C; (e) connected pore structure; (f) typical 3D-framework.

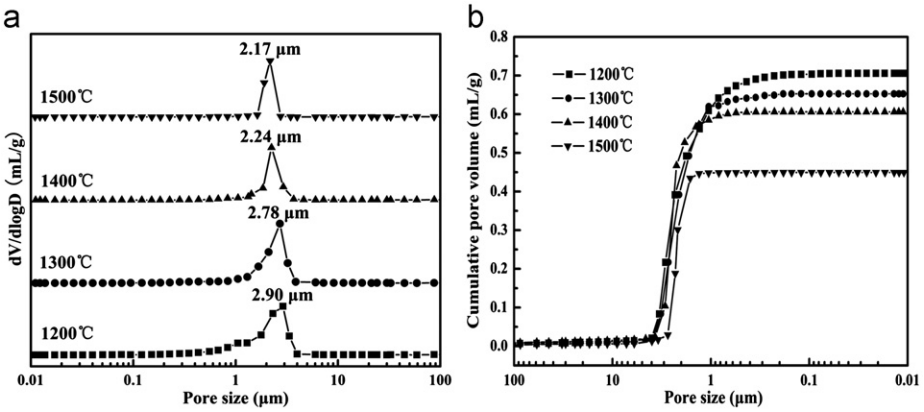

Fig. 9. Pore size distribution (a) and cumulative pore volume (b) of the porous Y_2SiO_5 ceramics with 30 wt% solid loading sintered at different sintering temperatures.

by the initial solid loading. As can be detected from the Fig.7, when the solid loading increased, the porosity was found to decrease sharply. By setting the sintering temperature as 1400 °C, the porosity reduced from 66.70% to 50.01% and the bulk density increased from 1.00 to 1.84 g/cm^3 by increasing the solid loading from 20 to 50 wt%. Fig.11 shows the pore structures after sintering at 1400 °C with different solid loadings varying from 20 to 50 wt%. It can be observed that the interconnected pores were homogeneously dispersed in the Y_2SiO_5 matrix and the adjacent particles interconnected,

forming a strong skeleton. With increasing solid loading, there would be more Y_2SiO_5 particles to take over the space of TBA solvent, resulting in an increase in bulk density and a decrease in porosity. The main properties i.e., compressive strength and room-temperature conductivity of porous Y_2SiO_5 ceramics sintered at 1400 °C with different solid loadings are illustrated in Fig. 12. As the initial solid loading increased, the compressive strength and the room-temperature conductivity increased from 3.43 to 24.45 MPa and from 0.08 to 0.55 W/m K, respectively. By adjusting the initial solid loading and sintering temperature, light weight Y_2SiO_5 ceramics with controlled microstructures and properties were prepared. It should be noted that the porous Y_2SiO_5 ceramics with 30 wt% solid loading and sintering at 1400 °C had an open porosity of 61.80%, a pore size of 2.24 μm, a low room-temperature thermal conductivity of 0.17 W/m K and a relative high compressive strength of 13.91 MPa, which makes this Y_2SiO_5 suitable for applications in thermal insulators.

4. Conclusion

Pure single-phase Y_2SiO_5 powder was prepared by calcining the Y_2O_3 and spherical SiO_2 powder mixtures at 1500 °C for 2 h without any additives. Highly porous Y_2SiO_5 ceramics with homogeneous 3D interconnected pore structures (with a pore size of 2～3 μm) were prepared by the novel TBA-based gel-casting. The formation

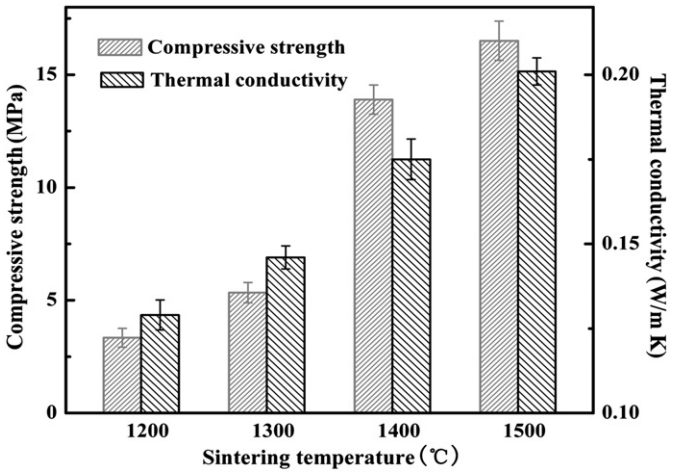

Fig. 10. Influence of sintering temperature (30 wt% solid loading) on compressive strength and room-temperature conductivity.

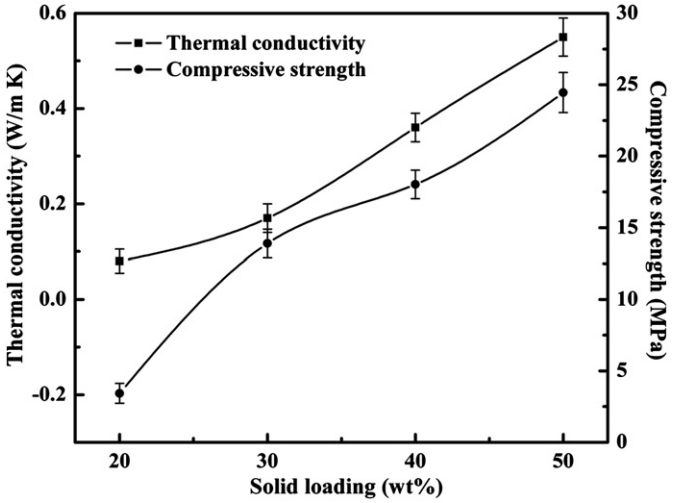

Fig. 12. Properties of porous Y_2SiO_5 ceramics sintered at 1400 °C with different solid loadings.

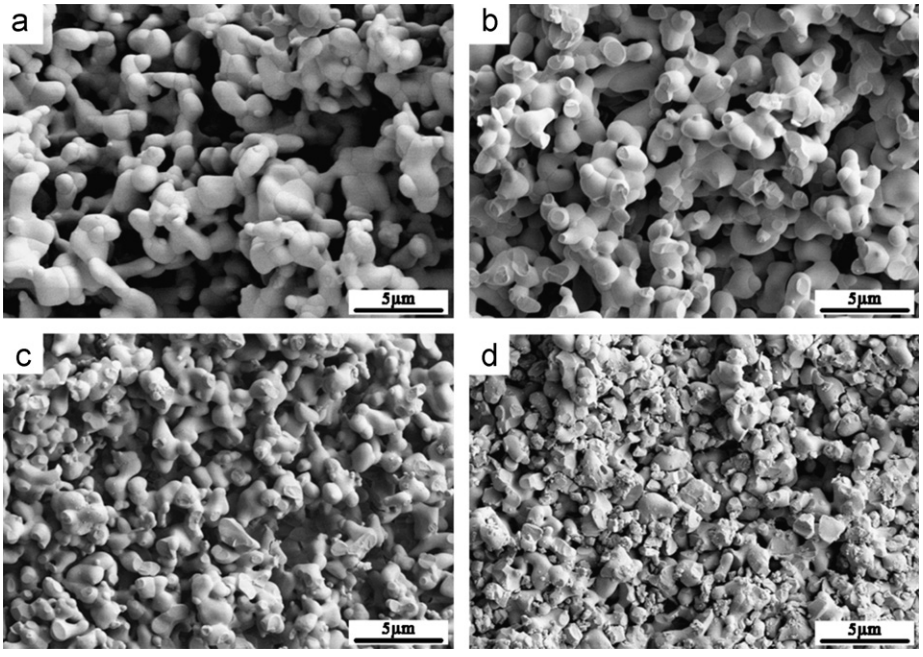

Fig. 11. Structure of pores in the porous Y_2SiO_5 samples sintering at 1400 °C with different solid loadings: (a) 20 wt%; (b) 30 wt%; (c) 40 wt%; (d) 50 wt%.

mechanism of special pore structure and the properties of the green body were discussed.

It is indicated that the properties of sintered porous Y_2SiO_5 ceramics were significantly influenced by the initial solid loadings and sintering temperatures. As the temperature increased from 1200 to 1500 °C the porosity and the pore size (for 30 wt% solid loading) decreased from 67.09% to 58.31% and from 2.90 to 2.17 μm, respectively. Correspondingly, the compressive strength increased from 3.43 to 24.45 MPa. As the solid loading increased from 20 to 50 wt%, the porosity(for 1400 °C) decreased from 66.70% to 50.01%, while the thermal conductivity increased from 0.08 to 0.55 W/m K, respectively.

It can be concluded that the porous Y_2SiO_5 ceramics fabricated by TBA-based gel-casting had a low thermal conductivity and relatively high compressive strength, indicating its applications in the high-temperature thermal insulators.

Acknowledgment

The authors would like to acknowledge the National Natural Science Foundation of China (Project No. 51172156) for financial support. The authors are also thankful to Professor Yanchun Zhou for his advice during the experiment process.

References

[1] A. Ito, J. Endo, T. Kimura, T. Goto, Eggshell- and fur-like microstructures of yttrium silicate film prepared by laser chemical vapor deposition, Materials Chemistry And Physics 125 (2011) 242–246.
[2] M. Liu, J.F. Huang, Y.T. Zhang, F. Deng, L.Y. Cao, J.P. Wu, Phase, Microstructure, and oxidation resistance of yttrium silicates coatings prepared by a hydrothermal electrophoretic deposition process for C/C composites, Journal Of Coatings Technology And Research 6 (2008) 531–535.
[3] M. Aparicio, A. Durán, Yttrium silicate coatings for oxidation protection of carbon-silicon carbide composites, J, Am. Ceram. Soc. 83 (2000) 1351–1355.
[4] J.F. HuangLi, H.J. Zeng, X.R. Li, K. Zhi, Yttrium silicate oxidation protective coating for SiC coated carbon/carbon composites, Ceramics International 32 (2006) 417–421.
[5] J.F. Huang, X.R. Zeng, H.J. Li, X.B. Xiong, Y.W. Fu, M. Huang, SiC/yttrium silicate multi-layer coating for oxidation protection of carbon/carbon composites, Journal Of Materials Science 39 (2004) 7383–7385.
[6] X.H. Zheng, Y.G. Du, J.Y. Xiao, W.J. Zhang, L.C. Zhang, Double layer oxidation resistant coating for carbon fiber reinforced silicon carbide matrix composites, Applied surface science 255 (2009) 4250–4254.
[7] H.J. Seifert, S. Wagner, O. Fabrichnaya, H.L. Lukas, F. Aldinger, T. Ullmann, M. Schmucker, H. Schneider, Yttrium silicate coatings on chemical vapor deposition-SiC-precoated C/C-SiC: Thermodynamic assessment and high-temperature investigation, Journal of the American Ceramic Society 88 (2005) 424–430.
[8] C. Argirusis, T. Damjanović, G. Borchardt, Yttrium silicate coating system for oxidation protection of C/C–Si–SiC composites: Electrophoretic deposition and oxygen self-diffusion measurements, Journal of the European Ceramic Society 27 (2007) 1303–1306.
[9] J.W. Nowok, J.P. Kay, R.J. Kulas, Thermal expansion and high-temperature phase transformation of the yttrium silicate Y_2SiO_5, Journal of materials research 16 (2001) 2251–2255.
[10] K. Fukuda, H. Matsubara, Anisotropic thermal expansion in yttrium silicate, Journal of materials research 18 (2003) 1715–1722.
[11] Z.Q. Sun, J.Y. Wang, M.S. Li, Y.C. Zhou, Mechanical properties and damage tolerance of Y_2SiO_5, Journal Of The European Ceramic Society 28 (2008) 2895–2901.
[12] Z.Q. Sun, M.S. Li, Y.C. Zhou, Thermal properties of single-phase Y_2SiO_5, Journal Of The European Ceramic Society 29 (2009) 551–557.
[13] Z.Q. Sun, Y.C. Zhou, M.S. Li, Effect of $LiYO_2$ on the synthesis and pressureless sintering of Y_2SiO_5, Journal of materials research 23 (2011) 732–736.
[14] L.F. Hu, C.A. Wang, Y. Huang, Porous yttria-stabilized zirconia ceramics with ultra-low thermal conductivity, Journal Of Materials Science 45 (2010) 3242–3246.
[15] J.H. Kim, J.H. Lee, T.Y. Yang, S.Y. Yoon, B.K. Kim, H.C. Park, TBA-based freeze/gel casting of porous hydroxyapatite scaffolds, Ceramics International 37 (2011) 2317–2322.
[16] T.Y. Yang, J.M. Lee, S.Y. Yoon, H.C. Park, Hydroxyapatite scaffolds processed using a TBA-based freeze-gel casting/polymer sponge technique, J. Mater. Sci. - Mater. Med 21 (2010) 1495–1502.
[17] Q. Fu, E. Saiz, A.P. Tomsia, Bioinspired strong and highly porous glass scaffolds, Advanced Functional Materials 21 (2011) 1058–1063.
[18] G.B. Wei, P.X. Ma, Nanostructured biomaterials for regeneration, Advanced Functional Materials 18 (2008) 3568–3582.
[19] A.K. Yang, C.A. Wang, R. Guo, Y. Huang, Microstructure and electrical properties of porous PZT ceramics fabricated by different methods, Journal of the American Ceramic Society 93 (2010) 1984–1990.
[20] L.N. Wu, Y.D. Huang, Z.J. Wang, L. Liu, Controlled fabrication of porous Al_2O_3 ceramic by N,N′-dimethylformamide-based gel-casting, Scripta Materialia 62 (2010) 602–605.
[21] S.A. Barr, E. Luijten, Structural properties of materials created through freeze casting, Acta materialia 58 (2010) 709–715.
[22] C. Vakifahmetoglu, P. Colombo, A direct method for the fabrication of macro-porous SiOC ceramics from preceramic polymers, Advanced Engineering Materials 10 (2008) 256–259.
[23] I.Y. Guzman, Certian principles of formation of porous ceramic structures. properties and aplications (a review), Glass and Ceramics 60 (2003) 280–283.
[24] P. Colombo, C. Vakifahmetoglu, S. Costacurta, Fabrication of ceramic components with hierarchical porosity, Journal Of Materials Science 45 (2010) 5425–5455.
[25] C.Q. Hong, X.H. Zhang, J.C. Han, J.C. Du, W. Zhang, Camphene-based freeze-cast ZrO_2 foam with high compressive strength, Materials Chemistry And Physics 119 (2010) 359–362.
[26] J.L. Yu, H.J. Wang, J. Zhang, D.H. Zhang, Y.L. Yan, Gelcasting preparation of porous silicon nitride ceramics by adjusting the content of monomers, Journal Of Sol-Gel Science And Technology 53 (2009) 515–523.
[27] R.F. Chen, Y. Huang, C.A. Wang, J.Q. Qi, Ceramics with ultra-low density fabricated by gelcasting: an unconventional view, Journal of the American Ceramic Society 90 (2007) 3424–3429.
[28] R.F. Chen, C.A. Wang, Y. Huang, L.G. Ma, W.Y. Lin, Ceramics with special porous structures fabricated by freeze-gelcasting: using tert-butyl alcohol as a template, Journal of the American Ceramic Society 90 (2007) 3478–3484.
[29] H. Xu, J.C. Liu, A.R. Guo, H.Y. Du, Z.G. Hou, Porous silica ceramics with relatively high strength and novel bi-modal pore structure prepared by a TBA-based gel-casting method, Ceramics International 38 (2012) 1725–1729.
[30] A.K. Yang, C.A. Wang, R. Guo, Y. Huang, Effects of porosity on dielectric and piezoelectric properties of porous lead zirconate titanate ceramics, Applied physics letters 98 (2011) 152904.
[31] R.F. Chen, Y. Huang, C.A. Wang, J.Q. Qi, Ceramics with ultra-low density fabricated by gelcasting: an unconventional view, Journal of the American Ceramic Society 90 (2007) 3424–3429.
[32] H. Xu, H.Y. Du, J.C. Liu, A.R. Guo, Preparation of sub-micron porous yttria-stabilized ceramics with ultra-low density by a TBA-based gel-casting method, Chemical Engineering Journal 173 (2011) 251–257.